Applied Catalysis B: Environmental 259 (2019) 118081

Contents lists available at ScienceDirect

Applied Catalysis B: Environmental

journal homepage: www.elsevier.com/locate/apcatb

C—O cleavage of diphenyl ether followed by C—C coupling reactions over hydrophobized Pd/HY catalysts

Cristiane A. Scaldaferri[a,b], Puridej Warakunwit[a], Vânya M.D. Pasa[b], Daniel E. Resasco[a,*]

[a] The University of Oklahoma, Center for Interfacial Reation Engineering (CIRE) and School of Chemical, Biological, and Materials Engineering, 100 East Boyd St., Norman, OK, 73019, USA

[b] Universidade Federal de Minas Gerais, Departamento de Química, Laboratório de Combustíveis, 6627 Antônio Carlos Ave, Belo Horizonte, MG, 31270-901, Brazil

ARTICLE INFO

Keywords:
Diphenyl ether
Lignin
C—C coupling products
Alkylation
Self-condensation
Bifunctional metal-acid catalyst
Biomass to fuels

ABSTRACT

The catalytic conversion of diphenyl ether (DPE), a dimeric model compound representing 4-O-5 lignin linkages, has been investigated using a hydrophobized bifunctional Pd/HY catalyst since the hydrophobicity of the catalyst significantly improved conversion and carbon balance. Partial hydrogenation of DPE was found to be an essential step before C—O bond cleavage and C—C bond formation, which are the target reactions in this study. The main products resulting from the C—O cleavage are phenol and cyclohexanone, which subsequently can undergo C—C coupling via alkylation and aldol condensation. The balance between hydrogenation activity of the metal and the acidic function of zeolite was found to play an important role for maximizing the yield of C—C coupling products, which are desirable in the upgrading of lignin-derived compounds to fuel components.

1. Introduction

Major bonds present in lignin include ether (β-O-4, α-O-4, and 4-O-5) and C—C (β-β, β-5, β-1 and 5-5) linkages [1–3]. Ether bonds are the most abundant group, constituting about 80% of the primary inter-unit linkages in the lignin structure. Among these bonds, the β-O-4 is predominant (30-50%), followed by α-O-4 (10-30%), with the specific percentages depending on the type of lignin. While the 4-O-5 bond is less abundant it is one of the strongest ether linkages, having a bond dissociation energy of 75.1 kcal/mol [3,4] and is more likely to remain intact during depolymerization and subsequent upgrading to fuels and chemicals [5–9]. Therefore, the target reactions on which we have concentrated our efforts in this paper are the cleavage of the 4-O-5 C—O bond and the subsequent formation of C—C bonds which is an attractive strategy to adjust the molecular weight of products to the range of fuels (particularly jet fuel and diesel).

Lignin has a very complex structure, so one of the approaches followed by researchers to facilitate the understanding of reaction pathways that ultimately may result in effective upgrading strategies has been the use of model compounds. Among them, several catalytic systems and different types of reactions have been investigated in recent years, using aromatic monomers (substituted benzylic alcohols) and/or dimers as model compounds to better understand the reactivity of the multifunctional groups present in the lignin structure, as well as some specific bonds, such as β-O-4, α-O-4, and 4-O-5, that can be cleaved during depolymerization reactions [4,10,11]. Typical model compounds used in the literature to explore the mechanisms of the C—O bond cleavage of lignin include 2-phenylethyl phenyl ether, benzyl phenyl ether and diphenyl ether, representing the breaking of β-O-4, α-O-4 and 4-O-5 linkages, respectively [4].

The selective hydrolytic cleavage of the arene-oxygen bond in aromatic ethers has been the subject of recent investigations [12,13]. For example, the mechanism derived from a study conducted on Pd/C catalysts implies that first the aromatic ring is partially hydrogenated to an enol ether and then the aromatic C—O bond is cleaved, with elimination of cyclohexanone and phenol [14].

Similarly, He et al. [15] have investigated the selective cleavage of ether linkages of aromatic ethers with β-O-4, α-O-4, and 4-O-5 bonds into monoaromatic molecules, which subsequently lead to the formation of hydrogenation products, such as cyclohexanol and cyclohexanone. These authors have observed the C—O -bond cleavage of benzyl phenyl ether in the presence of a bi-functional Ni/HZSM-5 catalyst. In this case, it was proposed that the presence of the metal plays an important role in the cleavage of the ether bond via hydrogenolysis while the acid function contributes to hydrolysis and alkylation reactions. The resulting yields of alkylated products were remarkably high (around 40%) [16], which is a very promising result for the conversion of lignin to jet fuel and diesel fuels. It has been recognized that after biomass depolymerization C—C coupling of phenolic compounds is an attractive strategy for adjusting the molecular weight of the resulting monomers

* Corresponding author.
E-mail address: resasco@ou.edu (D.E. Resasco).

https://doi.org/10.1016/j.apcatb.2019.118081
Received 18 February 2019; Received in revised form 3 August 2019; Accepted 12 August 2019
Available online 14 August 2019

to the required molecular weight range for fuel production [17–19]. Anaya et al. [20] have pointed out the importance of keeping a balanced acid/metal ratio in order to obtain high alkylation yields with phenolics compounds. That is, hydrogenation catalyzed by the metal is a necessary step for generating the alcohol, but excessive hydrogenation reduces the alkylation yield due to the consumption of the aromatic substrate needed in the reaction. Specifically, hydrogenation of *m*-cresol produces methylcyclohexanol, which is the precursor of the main alkylating agent (methylcyclohexene). However, only a fraction of *m*-cresol should be used to allow maximum alkylated products.

Likewise, aldol condensation reactions of oxygenated compounds such as furfurals and ketones have also been widely considered for the production of alkanes in the C8-C15 range from renewable sources such as xylose and fructose from cellulose [21–25]. These reactions are well known and are catalyzed by both bases and acids [26,27]. Relevant to the present work, Kikhtyanin et al. [28] compared performance of different zeolites for the aldol condensation of furfural and ketones. They found that despite having different acidity strengths, surface areas, and structures, HZSM-5, HBEA, HY and HMOR, all exhibited good activity for aldol condensation.

In acid-catalyzed reactions on zeolites, water usually has an adverse effect on activity, due to its competitive adsorption on the acid sites [29–32] or attack of the zeolite structure at high enough temperatures [31]. Tolerance to water can be improved by surface functionalization of the material with organosilane groups, which impart a hydrophobic character to the zeolite and minimizes the water attack. For example, Zapata et al. [32] have shown that alkylation of phenolic compounds can be conducted in biphasic systems with minimal degradation using hydrophobized HY zeolites. The crystallinity of the zeolite without functionalization was completely lost after a couple hours in hot liquid water, while the loss of crystallinity was much less when a functionalized zeolite was used. In addition, a lower deactivation rate was observed in a biphasic system. Thus, taking into account that water is ubiquitous in biomass processing and, even when an organic solvent is used, water is always an important byproduct of the C—C bond forming reactions, a hydrophobic 1% Pd/OTS-HY sample was selected as a catalyst in this study.

In the present study, we have explored the selective cleavage of the C—O bond of diphenyl ether, a typical 4-O-5 bond lignin model compound, combined with C—C coupling reactions (alkylation and aldol condensation) for the formation of products with desirable molecular weight for fuel applications. This work presents several experiments in order to provide new insights on diphenyl ether reaction pathways over Pd/OTS-HY and how the balance between metal and acid functions can control the resulting products. We have found that a combination of metal and acid functions is desirable to achieve C—O bond cleavage and, at the same time, formation of C—C bonds. Therefore, the hybrid catalyst employed in this study (Pd/OTS-HY) incorporates the three desirable functions: metallic function for hydrogenation, acid function for C—O cleavage reactions as well as C—C coupling reactions (both alkylation and aldol condensation), and a hydrophobic function for reducing catalyst deterioration.

2. Experimental

2.1. Catalyst preparation

The HY zeolite (CBV760 from Zeolyst, Si/Al ratio = 30, S (BET) = 734 m^2/g) and amorphous silica (HiSil, SiO_2) were used as provided. Zeolite Y was selected due to its 3-dimensional pore structure and high acid density [20], two desirable properties for alkylation and aldol condensation. Bifunctional HY-supported Pd catalysts were prepared by incipient wetness impregnation (IWI) with an aqueous solution of $Pd(NO_3)_2.2H_2O$ (Sigma-Aldrich), at varying metal loadings (0.1, 0.5, and 1.0%). Likewise, the SiO_2-supported Pd catalyst was prepared by IWI with aqueous nitrate solution, with a Pd loading of 2.0 wt %. In a typical catalyst preparation, 5 g of support was dried overnight in the oven at 383 K. Subsequently, a fresh aqueous solution of palladium nitrate was prepared, and slowly dropped onto the support. After impregnation, the catalyst was air-dried in the oven at 393 K for 12 h before calcined in air at 673 K for 4 h (2 K/min ramp).

Octadecyltrichorosilane (OTS) from Sigma-Aldrich, purity > 99%, was used to prepare hydrophobic zeolites (Pd/OTS-HY). For this purpose, the Pd-HY catalysts were dispersed in 100 mL of toluene using a Horn sonicator for 30 min at 40% of amplitude. The suspension of the Pd-HY particles was added to a solution of 1 mL of the sylilation agent (OTS) in 250 mL of toluene and stirred for 24 h at 500 rpm and 303 K. The hydrophobic catalyst was filtered, washed four times with ethanol, and dried overnight at 383 K. The resulting silane/zeolite ratio was 0.5 mmol/g.

In some reactions, physical mixtures of Pd/SiO_2 and OTS-HY catalysts were used at varying Pd/H^+ ratios to compare with the results obtained on the bifunctional Pd/OTS-HY catalyst.

2.2. Catalyst characterization

Specific BET surface areas and BJH pore volumes were obtained from N_2 adsorption/desorption isotherms on a Micrometrics ASAP 2020 unit, degassing the samples for 6 hours at 473 K prior to analysis. Powder XRD (PXRD) patterns were recorded on a model 6000 Shimadzu diffractometer, with a Cu tube, 30KV voltage, 30 mA current and a scanning speed of 1°/min in a 2θ range of 5° to 80°.

The acid density of the bare HY (Si/Al = 30), functionalized HY, and metal-loaded zeolites was estimated by IR analysis of pyridine adsorption. For these measurements, about 10 mg of sample was heated at 473 K for 2 h in N_2 flow (80-100 mL/min) in a tubular oven. Subsequently, N_2 was passed through a trap containing pyridine for 1 h. The oven temperature was subsequently increased to 373 K under N_2 flow, by-passing the pyridine trap, for 1 h in order to remove any physisorbed pyridine. Finally, the FTIR spectra were recorded with adding 64 scans on a Spectrum RX Spectrometer using the ATR technique.

For microscopy analysis, the Pd catalyst was supported on the sample port using the dispersed powder on conductive double-sided adhesive tape prior to scanning electron microscopy (SEM) analysis. A carbon cover was applied to the samples prior to measurements. The images and compositional microanalysis of a given area and chemical maps obtained by X-ray dispersive energy spectroscopy (EDS) were acquired on a Quanta 200 FEI - FEG scanning microscope. For transmission electron microscopy (TEM), the samples were dispersed in isopropanol and sonicated by a horn sonicator (Cole-Parmer), operating at an amplitude of 25% for 10 min before deposition onto holey carbon-coated copper grids. The images were obtained on a Tecnai G2-12 - SpiritBiotwin FEI field emission system operated at 120 kV.

2.3. Catalytic activity

Catalytic activity was measured in a 50-mL batch stainless-steel autoclave reactor (Parr Corporation). In a typical run, a measured amount of catalyst was mixed with 20 mL of decalin in the reactor vessel, which was purged three times with N_2 and then pressurized in H_2 to 1.4 MPa. To fully reduce the metal, the temperature was increased to 473 K and held for 1 h at a stirring speed of 500 rpm. After the reduction step, 5 mL of a mixture of diphenyl ether (DPE) in decalin was injected from a pressurized feed cylinder. The pressure of the reactor was adjusted to 3.4 MPa with additional H_2. It took only a few minutes for the temperature to *re*-adjust to the reaction temperature. After reaction, the reactor was rapidly cooled down to room temperature. By this method, we minimize the time at which the reaction mixture is not exactly under the defined reaction conditions. The resulting liquid product was filtered and analyzed by GC–MS and GC-FID. More details on the reaction procedure are included in the Supplementary

information S1.

A Hewlett Packard 6890 GC-FID equipped with a DB-1701 column (60 m × 0.25 mm × 0.25 m) was used for product quantitative analysis, while a Shimadzu QP2010 GC–MS equipped with a ZB-1701 column (60 m × 0.25 mm × 0.25 µm) was used for product identification. Commercially available standards were used when possible to confirm the identity of the products and determine their response factors, as previously described by Wan et al. [33]. Toluene was used as a quantitative internal standard that allowed exact determination of carbon balances. The carbon balance (C balance), the carbon yield (C yield), and the selectivity for each product are calculated as follows:

$$Carbon\ Balance\ (\%) = \frac{moles\ of\ product\ obtained\ \times\ C\ number\ \times\ 100}{mol\ of\ diphenyl\ ether\ consumed\ \times\ C\ number\ of\ DPE} \quad (1)$$

$$Selectivity\ (\%) = \frac{moles\ of\ product\ A \times C\ number \times\ 100}{Total\ moles\ C\ of\ products\ obtained} \quad (2)$$

$$Carbon\ Yield\ (\%) = \frac{moles\ of\ products\ obtained\ \times\ C\ number\ \times\ 100}{moles\ of\ DPE\ fed\ \times\ C\ number\ in\ DPE\ 12)} \quad (3)$$

3. Results and discussion

3.1. Catalyst characterization

The physical properties of the catalysts investigated are summarized in Table 1. The BET surface area and pore volume of HY were 723 $m^2 g^{-1}$ and 0.23 $cm^3 g^{-1}$, respectively. The metal-doped zeolite (1%Pd/HY) exhibited values of surface area and pore volume close to those of HY, indicating that the impregnation procedure did not affect significantly the zeolite structure. The functionalized catalysts (OTS/HY) showed a slight decrease in surface area as well as pore volume. In this case the additional incorporation of Pd, particularly at higher loadings did result in a moderate loss of surface area and pore volume, indicating a small degree of pore plugging.

Fig. 1a shows the FTIR spectra of HY (nonfunctionalized) and OTS/HY (functionalized) catalysts. The latter exhibits two bands centered at 2854 and 2922 cm^{-1}, which are due to stretching of methyl and methylene groups (CH_3 and CH_2) of the saturated aliphatic chains present in OTS.

The spectra for the adsorbed pyridine on the various zeolite catalysts are compared in Fig. 1b. The band centered at 1547 cm^{-1} corresponds to the vibrational mode of the pyridinium ion (Py-H^+) adsorbed on a Brønsted site, while the one at 1442 cm^{-1} corresponds to pyridine coordinated with a Lewis site (Py -L). Finally, the band at 1490 cm^{-1} has contribution of both species. Clearly, both Brønsted and Lewis acid sites are present on all the catalysts. It is observed that, as indicated before [19,24], the Brønsted sites are not significantly reduced by the grafting of the organosilanes, while the Lewis sites are blocked to some extent. As previously shown [19,24] this is a beneficial aspect of the functionalization with chlorosilanes, which allows the HY zeolite to retain a large fraction of its alkylation and aldol-condensation activity since both reactions are catalyzed by Brønsted sites.

Table 1
Specific surface area and pore volume of the catalysts.

Catalysts	BET area ($m^2 g^{-1}$)	Pore volume ($cm^3 g^{-1}$)
HY	723	0.23
1%Pd/HY	748	0.23
OTS/HY	604	0.13
0.1%PdOTS/HY	609	0.18
0.5%PdOTS/HY	570	0.17
1%PdOTS/HY	514	0.16

The XRD patterns of the OTS functionalized and metal-doped catalysts are compared to those of the unfunctionalized zeolites (Fig. 2). It is observed that the relative intensities and positions of all the diffraction peaks show no distinguishable differences upon OTS or metal addition. This is another good characteristic of the functionalization with OTS, which does not degrade the zeolite crystallinity.

Similarly, the TEM and SEM images (Supplementary information S2) reveal well-ordered and uniform crystallites on both unfunctionalized and functionalized zeolites. The SEM/EDS chemical maps show a very homogeneous distribution of zeolite constituents and metal particles.

3.2. Catalytic activity measurements

3.2.1. Enhanced stability of hydrophobic Pd/OTS-HY catalysts

Table 2 compares the conversion and carbon balances obtained on the functionalized (1% Pd/OTS-HY) and unfunctionalized (1% Pd/HY) catalysts. Under all the reaction conditions investigated, the conversion on the functionalized 1% Pd/OTS-HY was significantly higher than on the unfunctionalized sample.

For the hydrophilic sample in the biphasic system, the presence of liquid water caused a significant loss in reaction rate, which was anticipated from previous work [31]. Interestingly, an activity difference was also observed in the organic solvent, which as mentioned above may be related to the effect of water generated during the C—C bond forming reaction. The carbon balance was about the same for the two catalysts when the reaction was conducted in single organic solvent. The apparent differences in carbon balance observed for the biphasic reactions may simply be a consequence of the much lower degree of conversion in the unfunctionalized catalyst. It is then clear that the performance of the catalyst functionalized with organosilanes is better than that of unfunctionalized catalysts in both, biphasic and single organic phase systems.

3.2.2. Product distribution and reaction pathways

The distribution of products from the conversion of diphenyl ether as a function of catalyst mass for 1 h reaction at 473 K in the presence of 3.4 MPa H_2 is shown in Fig. 3. This analysis allows us to evaluate the evolution of products as a function of the extent of reaction. When operating in a batch reactor with potential catalyst deactivation, instead of following the product distribution as a function of time, it is preferred to follow the evolution as a function of catalyst mass with constant (short) reaction time. With this method, one can identify primary and secondary products, as we would typically do when following the evolution of products as a function of time.

Accordingly, as shown in Fig. 3, several compounds would appear as primary products by showing non-zero slopes when the extent of reaction approaches zero. However, one may not expect that all of them are primary products. Specifically, cyclohexane and cyclohexanone, as well as all bicyclic compounds, such as [1'-bicyclohexyl]-2-one, 2-cyclohexylphenol, and 4-cyclohexylphenol, grouped together as carbon-carbon coupling products, require an initial hydrogenation step and cannot be primary products.

Also, as shown below, without hydrogenation the ether cannot be cleaved. In fact, as proposed in Fig. 4, the primary product should be cyclohexylphenyl ether (CPE), the partial hydrogenation product from DPE. Subsequent cleavage of the C—O bond leads to the formation of phenol/cyclohexene or cyclohexanone/benzene. The low concentration of benzene observed would indicate that the latter cleavage is less favored than the former. As the reaction progresses, cyclohexanone can undergo self-aldol condensation as well as hydrogenation/alkylation that result in the formation of the observed C—C coupling products with parallel decrease of cyclohexanone and phenol, as observed in Fig. 3. One can note that particularly at the lowest conversions, the sum of oxygenates (cyclohexanone + phenol) exceeds that of non-oxygenates (benzene + cyclohexane), which may be due to preferential

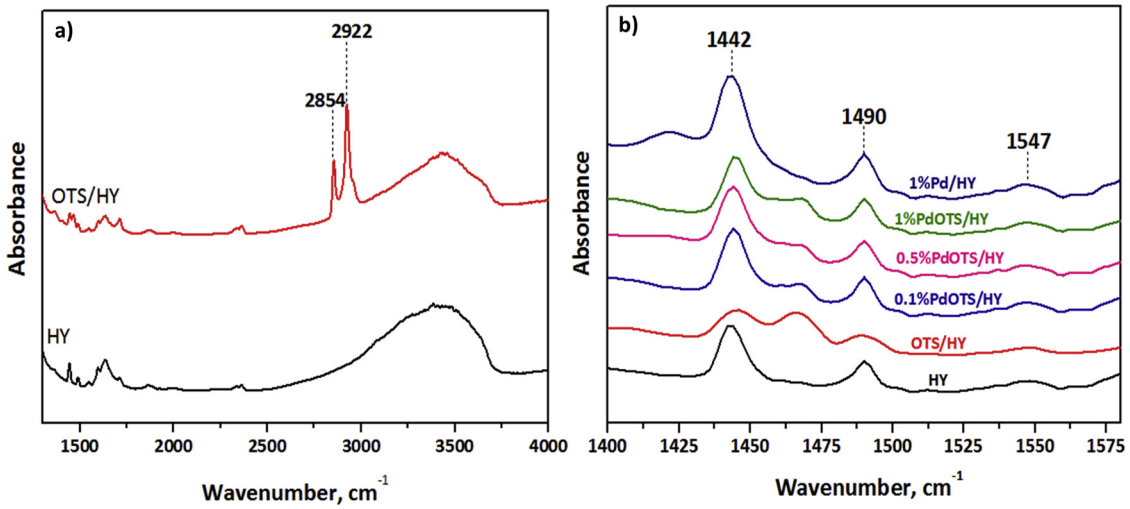

Fig. 1. a) FTIR spectra (1500-4000 cm^{-1}) of functionalized (OTS/HY) and non-functionalized (HY) zeolites pretreated at 473 K for 2 hours in N_2 flow (80-100 mL/min; **b)** FTIR spectra (1400-1600 cm^{-1}) after pyridine chemisorption on acid sites. After the initial pretreatment, the sample was cooled down to 323 K and the flow of N_2 directed to a trap containing pyridine to expose the catalysts to the adsorbate for 1 h. Then, the oven temperature was increased to 373 K under pure N_2 flow to remove any physisorbed pyridine. For each Spectrum 32 scans were recorded with on a Spectrum RX Spectrometer using the ATR mode.

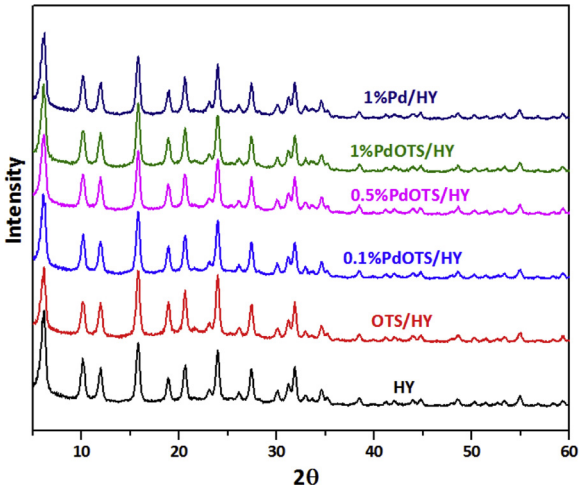

Fig. 2. X-ray diffraction (XRD) of HY, OTS/HY, 0.1%PdOTS/HY, 0.5%PdOTS/HY, 1%PdOTS/HY and 1%Pd/HY.

evaporation losses before analysis of the more volatile non-oxygenated compounds, which causes a more pronounced relative error with lower product yields.

3.2.3. Catalyst functions in Pd/OTS-HY

To differentiate the roles of the acid sites and metal sites in the bifunctional catalyst, monofunctional 2% Pd/SiO_2 (metallic) and OTS/HY (acid) catalysts were used to evaluate the performance of the metal and acid sites, separately. The product distribution, conversion level, and carbon balance for the different catalysts are summarized in Tables 3 and 4. Clearly, on the monofunctional 2% Pd/SiO_2 catalyst the dominant reaction is hydrogenation of the diphenyl ether to cyclohexylphenyl ether (CPE) and dicyclohexyl ether (DCE). Products derived from the cleavage of the ether linkage (cyclohexane, benzene, cyclohexanol, cyclohexanone and phenol) were observed to a much lesser extent compared to the extent of cleavage observed on the bifunctional catalyst. For instance, the selectivity to C6 compounds on Pd/SiO_2 was around 22% while that on Pd/OTS-HY was 63.5%. At the same time, no activity under identical reaction conditions was observed on the monofunctional OTS/HY acid catalyst (Table 4), which indicates that without a prior hydrogenation the HY zeolite alone is unable to cleave the O—C_{arom} bond of the DPE molecule. Thus, the partial hydrogenation of the aromatic ring at the metal site must occur in order to obtain C6 compounds, which requires the presence of metal sites, such as Pd. By contrast, the metal alone has very low activity for C—C cleavage, even on the hydrogenated compound and, of course, the C—C coupling reactions (alkylation and aldol condensation) only occur on the acid sites. Therefore, it can be concluded that a bifunctional catalyst is necessary for the desirable DPE conversion to fuel range molecules.

In fact, a similar sequential conversion path involving a C_{aliph}-O-bond cleavage followed by alkylation has been previously observed in the upgrading of biomass-derived compounds and described by Zhu et al. [34], who reported the conversion of methoxybenzene, containing an ether linkage over a Pt/Hbeta zeolite. In that study, it was shown that after the cleavage of the methoxy group (O-CH_3), the methyl group left on the surface was transalkylated to the aromatic ring of phenol to produce cresol and to the ring of unconverted anisole to produce methylanisole. These results give further support to the reaction pathway proposed in Fig. 4, which imply that the first step is partial hydrogenation of DPE at the metal site to form cyclohexylphenyl ether (CPE), while cleavage of the C—O bond on this compound is predominantly

Table 2
Comparison of DPE conversion (%) and carbon balance (%) of 1% PdOTS/HY and 1% Pd/HY in (a) the organic phase system and (b) a biphasic system.

Catalyst	DPE Conversion in organic phase (%)	DPE Conversion in biphasic system (%)	Carbon balance in organic phase (%)	Carbon balance in biphasic system (%)
1% PdOTS/HY	98	47	80	88
1% Pd/HY	75	5	73	96

(a) Reaction conditions in the organic phase: diphenyl ether concentration (0.15 M), decalin (25 mL), 473 K, 3.4 MPa of H_2, 1 h, stirring speed of 500 rpm. Catalyst reduction: 473 K, 1.4 MPa of H_2, 1 h, stirring speed of 500 rpm. Catalyst amount: 60 mg.
(b) Reaction conditions in biphasic system: diphenyl ether concentration (0.15 M), decalin (12.5 mL), water (12.5 mL) 473 K, 3.4 MPa of H_2, 1 h, stirring speed of 500 rpm. Catalyst reduction: 473 K, 1.4 MPa of H_2, 3 h, stirring speed of 500 rpm. Catalyst amount: 60 mg.

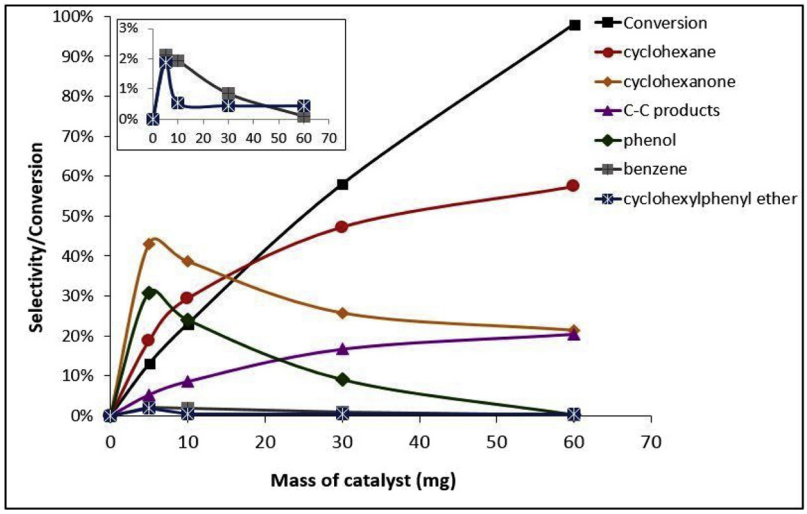

Fig. 3. Product distribution for the conversion of diphenyl ether over 1% PdOTS/HY catalyst as a function of catalyst mass. Reaction conditions: diphenyl ether concentration (0.15 M), decalin (25 mL), 473 K, 3.4 MPa H_2, 1 h, stirring speed of 500 rpm.

catalyzed by the acid sites. As show in Table 5, the main products from this cleavage are phenol and cyclohexene, which indicates that the C—O bond breaking preferentially occurs at the C_{aliph}-O-bond, which is in line with the finding that the C_{arom}-O bond cleavage does not occur in DPE. In a recent study, Guo et al. [35] found that PdRu bimetallic nanoparticles were active for the C—O cleavage in the conversion of diphenyl ether. In that catalyst an acid site was not required since Pd provided the hydrogenation activity while Ru was able to catalyze the C—O bond cleavage. This is consistent with our previous study on m-cresol conversion in which we demonstrated that while on Pd and Pt the cleavage of the C—O bond has a very high activation barrier on Ru the barrier is much lower [36].

3.2.4. Inter- and intra-molecular pathways for C—C coupling

In addition to the formation of bicyclic products via the hydrogenation/cleavage/C-—C coupling route shown in Fig. 4, one could consider the possibility of an intra-molecular, in which the C—O cleavage and the C—C bond forming reactions occur in a concerted way on the same molecule. To quantify the maximum extent to which this reaction pathway may participate in the overall conversion of DPE a series of separate reaction experiments were conducted.

For this series, *m*-cresol was added to the DPE feed. By including a separate single-ring molecule with a methyl tag to identify its products, we can compare the production of C-C coupling products exhibiting the methyl tag with those which do not have it. Clearly, illustrated in Fig. 5, those with the tag must arise from *m*-cresol, which can only be alkylated in an inter-molecular reaction. Those without the methyl tag may have been formed by either inter- or intra-molecular conversion.

Specifically, 2-cyclohexylphenol (compound A) and its hydrogenated derivative [1,1'-bi(cyclohexan)]-2-one (compound B) could form by either direct (intra-molecular) rearrangement of CPE or by $C_{aliphatic}$-O- cleavage of CPE with subsequent phenol alkylation. By contrast, when *m*-cresol is present, 2-cyclohexyl-5-methyl phenol (compound C) and its hydrogenated derivative {4-methyl-[1,1'-bi(cyclohexan)]-2-one} (compound D) are formed by inter-molecular alkylation.

To quantify the contribution of each pathway, we conducted several runs at varying *m*-cresol/DPE molar ratios (0, 0.25, 0.5, 1.0) while maintaining the DPE concentration constant (0.15 M). We anticipate that if the intra-molecular rearrangement were a dominant pathway, compounds C (and D), which can only occur inter-molecularly would be much less than compound A (and B), which can occur by both inter-

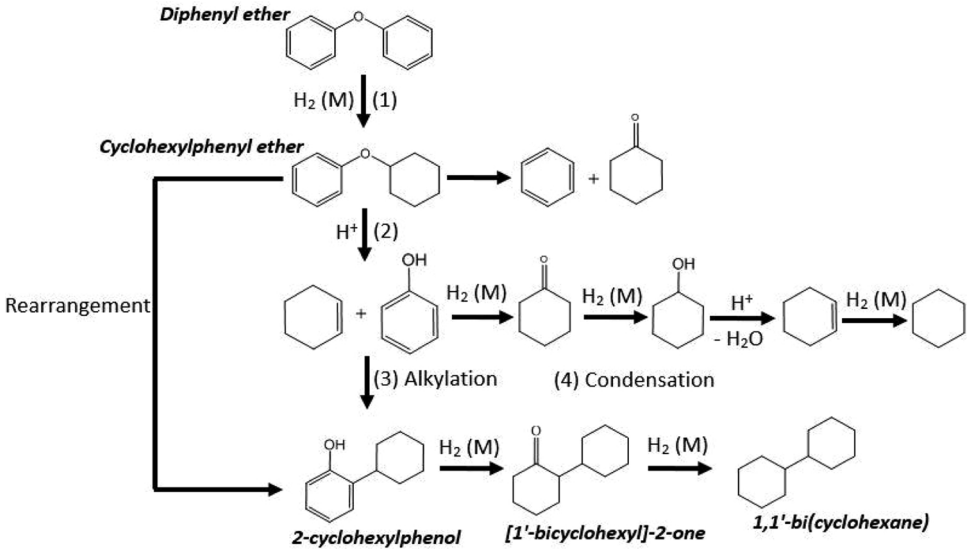

Fig. 4. Proposed pathways for the conversion of diphenyl ether over PdOTS/HY catalyst. H_2 (M): hydrogenation on a metal site. H^+: reaction on an acid site.

Table 3
Product distributions from diphenyl ether over 1% PdOTS/HY and 2% Pd/SiO_2 catalysts. Reaction conditions: diphenyl ether concentration (0.15 M), decalin (25 mL), 473 K, 3.4 MPa of H_2, 1 h, stirring speed of 500 rpm.

Products	[a]2%Pd/SiO_2		[b]1%PdOTS/HY	
	C Selectivity (%)	C Yield (%)	C Selectivity (%)	C Yield (%)
	3.53	2.96	47.38	36.04
	1.45	1.22	0.00	0.00
	7.59	6.35	0.00	0.00
	9.64	8.06	17.47	13.29
	0.23	0.19	0.23	0.17
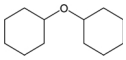	47.85	40.03	0.00	0.00
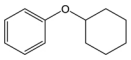	29.71	24.85	1.64	1.25
	0	0	28.94	23.41
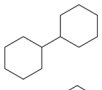	0	0	2.56	1.95
	0	0	1.42	1.08
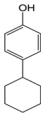	0	0	0.37	0.28

[a] Catalyst amount: 100 mg; conversion: 98.75 and C balance: 86.32%.
[b] Catalyst amount: 60 mg; conversion: 97.64% and C balance: 80.31%.

Table 4
Total carbon yield (C yield), conversion and carbon balance (C balance) for the reactions from diphenyl ether over 60 mg OTS/HY, 60 mg 1% PdOTS/HY and 100 mg 2% Pd/SiO_2 catalysts. Reaction conditions: diphenyl ether concentration (0.15 M), decalin (25 mL), 473 K, 3.4 MPa of H_2, 1 h, stirring speed of 500 rpm.

Catalyst	OTS/HY	1% PdOTS/HY	2%Pd/SiO_2
Total C yield (%)	0	76	84
Conversion (%)	0	98	99
C balance	90	80	86

and intra-molecular pathways. Moreover, by varying the amount of *m*-cresol while keeping DPE constant, we can observe the variation of the (C + D)/(A + B) molar ratio as the amount of *m*-cresol increased.

As shown in Table 6, compounds C and D were dominant when the *m*-cresol/DPE ratio was near unity, indicating that alkylation reactions occurred to a significantly higher extent than the intra-molecular rearrangement. Unfortunately, it was observed that the overall DPE conversion decreased with increasing the *m*-cresol/DPE ratio, which makes a complete quantification uncertain. This decrease in activity is probably due to the inhibition of the metal activity by the presence of excess *m*-cresol, which may strongly compete for adsorption metal sites, thus reducing the initial hydrogenation step.

In the conversion of DPE, 2-cyclohexylphenol (ortho) was observed as a C-C major product, with 4-cyclohexylphenol (para) to a lower extent and no 3-cyclohexylphenol (meta). This distribution is consistent with that expected from phenol alkylation, an electrophilic aromatic substitution with cyclohexene as alkylating agent, [37–39] and catalyzed by acid sites via carbenium ion [38–41].

3.2.5. C—C coupling via acid-catalyzed aldol condensation

Another C—C coupling reaction that could also occur in this system is the self-condensation of cyclohexanone (Supplementary information S3) that yield first the 1'-hydroxy-[1,1'-bi(cyclohexan)]-2-one, which can subsequently undergo to dehydration to [1,1'-bi(cyclohexan)]-1'-en-2-one and further hydrogenation to [1,1'-bi(cyclohexan)]-2-one [42], which is experimentally observed (Tables 3 and 7).

To quantify the significance of this reaction in the overall reaction pathway, we conducted an additional reaction experiment cofeeding cyclohexanone and *m*-cresol over the 1% Pd/OTS-HY catalyst. Two types of different C—C products are expected, depending on the extent of self-condensation and alkylation reactions. That is, the former should produce C12 compounds from two C6 reactants, while the latter C13 compounds from each C6 and C7 reactants. The distribution of the products and the respective selectivity data for this reaction are presented in Table 7.

Both C-C products [1,1'-bi(cyclohexan)]-2-one (C12) and 2-cyclohexyl-5-methylphenol (C13) products were obtained. However, the selectivity for the [1,1'-bi(cyclohexan)]-2-one (C12) was around five times greater (5.4%) than the selectivity for 2-cyclohexyl-5-methylphenol (C13) (1.0%). That is, the aldol condensation reaction of cyclohexanone seems to be dominant over the alkylation pathway. This poses a problem if one wants to maximize the production of C-C products from DPE. That is, if cyclohexanone is more rapidly consumed than the alkylation pathway, the selectivity to deoxygenated C6 products will always be dominant.

On this catalyst, it is observed that hydrogenation reactions occurred to a significantly greater extent than carbon-carbon coupling reactions, and high selectivity to single-ring saturated compounds is observed (Table 7), cyclohexane (49.3%), cyclohexanol (20.8%), methylcyclohexanone (20.6%). It is clear that the relative rate of hydrogenation is exceedingly high to maximize C-C products. Therefore, phenol is rapidly converted to cyclohexanone via ring hydrogenation, while the necessary carbonyl hydrogenation of cyclohexanone to cyclohexanol is slower. As a result, cyclohexanone accumulates, facilitating the self-aldol condensation. Since production of cyclohexanol is slow, alkylation of the remaining phenol is also slow, which favors further production of cyclohexanone instead of alkylation products.

3.2.6. Relative rates of the various hydrogenation steps

To investigate the relative hydrogenation rates, hydrogenation rate measurements of phenol and cyclohexanone were conducted under the same conditions. The initial reaction rates reported in Table 8 were obtained from analyzing data at varying conversion and extrapolation to initial concentration (zero conversion).

Clearly, the initial rate of phenol hydrogenation is much higher than that of cyclohexanone hydrogenation (7.6 fold). Therefore, as anticipated, once cyclohexanone is formed upon C-O cleavage, the subsequent hydrogenation to cyclohexanol, which should then be dehydrated to generate the alkylating agent cyclohexene, occurs at a much lower rate than the formation of cyclohexanone, which allows accumulation of this carbonyl compound, which leads to aldol-condensation. The cyclohexene that is formed (at a lower rate) is rapidly consumed in the alkylation reaction or further hydrogenated to cyclohexane, which explains why cyclohexene is not observed. Therefore, if one wants to maximize the alkylation reaction, the rate of hydrogenation should be controlled to a value high enough to start the reaction by saturating the first ring, however not so high to avoid all undesirable secondary hydrogenations. That is, while it was shown that

Table 5
Product distribution from cyclohexylphenyl ether conversion over (only acid) OTS/HY catalyst. Catalyst amount: 10 mg. Reaction conditions: cyclohexyl phenyl ether concentration (0.15 M), decalin (25 mL), 473 K, 3.4 MPa of N_2, 1 h, stirring speed 500 rpm. Conversion: 22%, C balance: 98%.

Products	Selectivity (%)	Carbon Yield (%)
	4.0	0.8
	46.2	8.9
	0.2	0.2
	4.4	0.8
	43.1	8.5
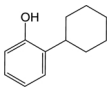	1.8	0.7
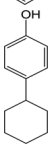	0.3	0.1

without hydrogenation the DPE conversion does not start, an excessive hydrogenation severely inhibits the yield to desirable C-C products.

3.2.7. Effect of varying the metal/acid site ratio

Since hydrogenation, alkylation and condensation are concurrent reactions maximizing C—C products requires to control the metal/acid site balance. To quantify this effect, the C-C/C6 product ratio, overall carbon yield and product distribution were compared in a series of Pd/OTS-HY catalysts with varying Pd loadings (0.1%, 0.5%, and 1% of Pd) as well as in a series of physical mixtures of catalysts containing the two functions separated (Pd/SiO_2 + OTS/HY).

Table 6
Products obtained by co-feeding diphenyl ether and *m*-cresol at varying ratios *m*-cresol/DPE over 60 mg of 1% PdOTS/HY catalyst. Molar ratios of 0, 0.25, 0.5, 1.0, with DPE concentration constant of 0.15 M. Reaction conditions: decalin (25 mL), 473 K, 3.4 MPa of H_2, 1 h, stirring speed of 500 rpm.

Molar ratio *m*-cresol/DPE	% C-C products yield from phenol (A + B)	% C-C products yield from *m*-cresol (C + D)	Molar ratio (C + D)/(A + B)
0	4.8	0	0
0.25	3.0	0.9	0.30
0.5	1.2	1.0	0.76
1	0.4	1.1	2.44

As shown in Fig. 6 for the three catalysts, the C-C/C6 product ratio initially increases with conversion and then reaches a plateau. As mentioned above, the C—C coupling is a secondary reaction that first requires hydrogenation and C—O cleavage. During the C—C coupling C6 products are converted into C12 products, which explains the increase in the product ratio. However, after a given DPE conversion has been reached, the ratio remains constant as both C—C and C6 products are formed at comparable rates. A more important observation for the discussion in this section is that as the Pd loading decreases, the C—C/C6 product ratio at which this plateau is reached becomes higher. Evidently, as proposed above, lowering the hydrogenation causes an enhancement in the C-C/C6 product ratio at any given DPE conversion. A very similar trend can be observed with physical mixtures of Pd/SiO_2 and OTS/HY catalysts. For example, when compared at the same overall DPE conversion a significantly higher C—C/C6 product ratio is observed for a mixture of Pd/H^+ molar ratio of 0.43 than for one with an equimolar Pd/H^+ ratio.

Fig. 7 further demonstrates this trend by showing that on the three catalysts, for a given yield of cyclohexane obtained (undesirable product), the yield of C—C products increases as the Pd loading is decreased. These results indicate that by adjusting the number of metal sites relative to the number of acid sites in the catalyst, it is possible to obtain a higher yield of carbon-carbon coupling products. As shown in Table 4, the Pd loading cannot be zero, but only a small amount of metal is enough to enhance the yield of C—C products.

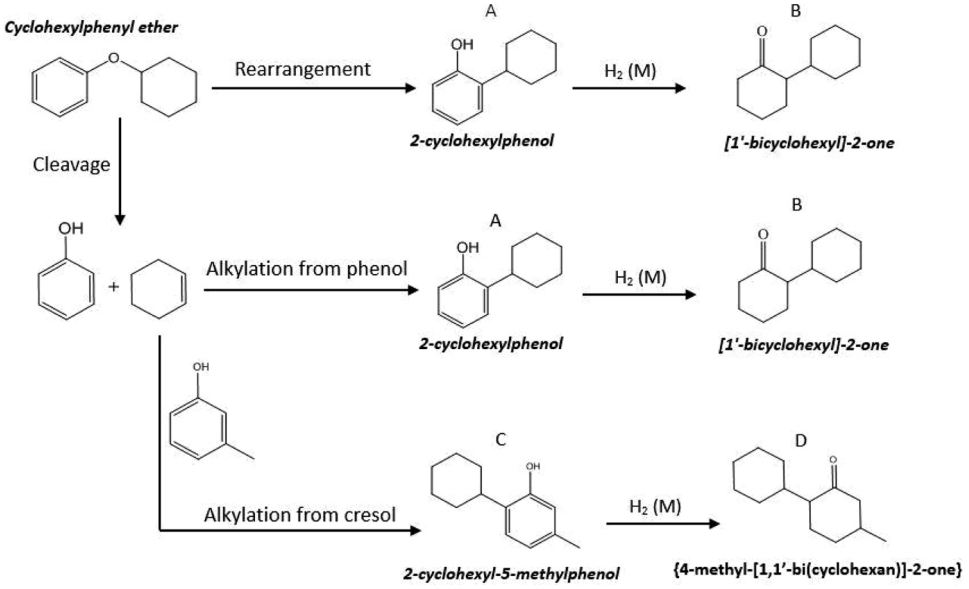

Fig. 5. Scheme for rearrangement and alkylation reactions when co-feeding diphenyl ether and *m*-cresol.

Table 7
Product distribution and selectivity for the reaction of *m*-cresol and cyclohexanone over 1%PdOTS/HY catalyst. Catalyst amount: 10 mg. Reaction conditions: cyclohexanone concentration (0.01 M), cresol concentration (0.01 M), decalin (25 mL), 473 K, 3.4 MPa of H_2, 1 h, stirring speed of 500 rpm. cresol conversion: 7%, cyclohexanone conversion: 17%, C balance: 89%.

Products						
Selectivity, %	49.3	20.8	2.9	20.6	5.4	1.0

Table 8
Reaction rates of phenol (r_1) and cyclohexanone (r_2) hydrogenation over 2% Pd/SiO_2 catalyst. Reaction conditions: Phenol concentration 0.45 M, or cyclohexanone concentration 0.4 M, in decalin solvent, total volume 25 mL, 473 K, 3.4 MPa H_2, 1 h reaction, constant stirring speed of 500 rpm.

Rate (mol/g_{cat}.hr)	0.46	0.06

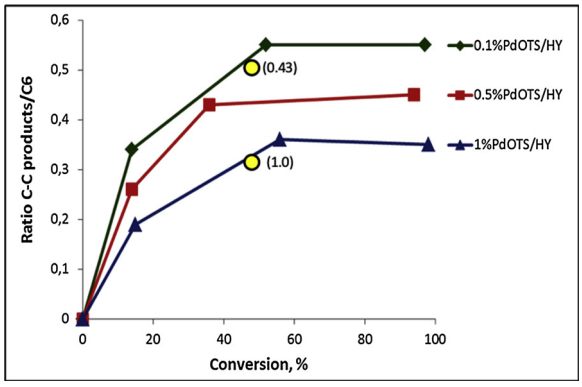

Fig. 6. Molar ratio of C-C products/C6 for the different loadings of Pd on PdOTS/HY catalyst as function of conversion. Reaction conditions: diphenyl ether concentration (0.15 M), decalin (25 mL), 473 K, 3.4 MPa of H_2, 1 h, stirring speed 500 rpm. Catalyst amount: 10, 30 and 60 mg. The two additional data points (circles with indicated numbers in parentheses), represent data from two physical mixtures of Pd/SiO_2 and OTS/HY with Pd/H^+ molar ratios of 0.43 and 1.0.

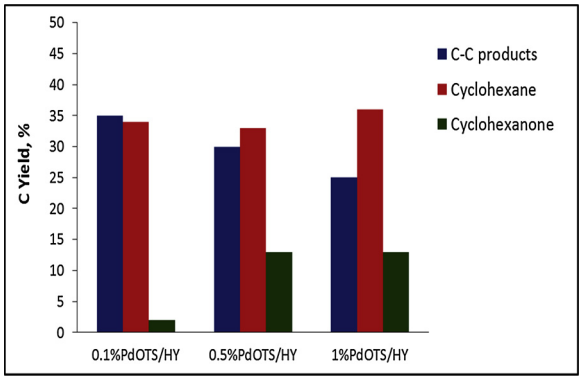

Fig. 7. Carbon yield of products obtained over different metal loadings on PdOTS/HY catalyst. Reaction conditions: diphenyl ether concentration (0.15 M), decalin (25 mL), 473 K, 3.4 MPa of H_2, 1 h, stirring speed of 500 rpm. Conversion: 97%, 94% and 98%.

4. Conclusions

The present study analyzes the various reaction pathways for the conversion of diphenyl ether, which is a typical 4-O-5 bond lignin model compound. A hydrophobized bifunctional Pd/OTS-HY catalyst has been used to investigate possible pathways catalyzed by a combination of the two catalytic functions (metal/acid). First, the hydrophobicity of the catalyst exhibits enhanced tolerance to water formed during the reaction and helps inhibiting catalyst deactivation. With the goal of achieving a maximum yield of carbon-carbon coupling products, the influence of each reaction has been investigated. It is demonstrated that without an initial hydrogenation, diphenyl ether cannot be efficiently converted. In this sense, Pd provides enough hydrogenation activity to partially hydrogenate diphenyl ether to the main primary product in the sequence, cyclohexylphenyl ether. The HY zeolite provides the acid function and selectively cleaves the C_{aliph}-O-bond in cyclohexylphenyl ether to get phenol and cyclohexene. Subsequently, phenol can be alkylated by cyclohexene, which arises from both, this cleavage and the hydrogenation/dehydration of cyclohexanone, which in turn is produced by ring hydrogenation of phenol. Since the hydrogenation/dehydration of cyclohexanone occurs at a lower rate than its rate of formation, this carbonyl molecule becomes the main source of C—C coupling products via self-aldol condensation. If the metal function is excessively active compared to the acid function, the yield of C—C products decreases. However, by adjusting the metal/acid function ratio, it is possible to enhance the yield of C—C products.

Declaration of Competing Interest

The authors declare that they have no known competing financial interests or personal relationships that could have appeared to influence the work reported in this paper.

Acknowledgements

Two of us (CAS and VMDP) acknowledge financial support from the Coordenação de Aperfeiçoamento de Pessoal de Nível Superior – CAPES and the Conselho Nacional de Desenvolvimento Científico e Tecnológico – CNPq (Brazil). Two of us (DER and PW) acknowledge financial support from the U.S. Department of Energy, Basic Energy Sciences (Grant DE-SC0018284).

Appendix A. Supplementary data

Supplementary material related to this article can be found, in the online version, at doi:https://doi.org/10.1016/j.apcatb.2019.118081.

References

[1] S. Gillet, M. Aguedo, L. Petitjean, A.R.C. Morais, A.M. da Costa Lopes, R.M. Lukasik, P. Anastas, Lignin transformations for high value applications: towards targeted modifications using green chemistry, Green Chem. (2017) 4200–4233, https://doi.org/10.1039/C7GC01479A.
[2] F.G. Calvo-Flores, J.A. Dobado, Lignin as renewable raw material, ChemSusChem 3 (2010) 1227–1235, https://doi.org/10.1002/cssc.201000157.
[3] M. Chatterjee, T. Ishizaka, H. Kawanami, Hydrogenolysis/hydrogenation of diphenyl ether as a model decomposition reaction of lignin from biomass in

pressurized CO2/water condition, Catal. Today. 281 (2017) 402–409, https://doi.org/10.1016/j.cattod.2016.02.050.
[4] X. Wang, R. Rinaldi, Solvent effects on the hydrogenolysis of diphenyl ether with raney nickel and their implications for the conversion of lignin, ChemSusChem. 5 (2012) 1455–1466, https://doi.org/10.1002/cssc.201200040.
[5] A. Yamaguchi, N. Mimura, M. Shirai, O. Sato, Effect of metal catalysts on bond cleavage reactions of lignin model compounds in supercritical water, Waste Biomass Valorization 0 (2019) 0, https://doi.org/10.1007/s12649-019-00647-4.
[6] B. Sedai, R.T. Baker, Copper Catalysts for Selective C À C Bond Cleavage of b -O-4 Lignin Model Compounds, (2014), https://doi.org/10.1002/adsc.201400463.
[7] J. Hu, S. Zhang, R. Xiao, X. Jiang, Y. Wang, Y. Sun, P. Lu, Catalytic transfer hydrogenolysis of lignin into monophenols over platinum- rhenium supported on titanium dioxide using isopropanol as in situ hydrogen source, Bioresour. Technol. 279 (2019) 228–233, https://doi.org/10.1016/j.biortech.2019.01.132.
[8] S. Liu, L. Bai, A.P. Van Muyden, Compounds with a Single-Atom Co Catalyst †, (2019), pp. 1974–1981, https://doi.org/10.1039/c9gc00293f.
[9] C. Ju, M. Li, Y. Fang, phenolic compounds over bifunctional catalysts with optimized acid / metal interactions †, Green Chem. (2018) 4492–4499, https://doi.org/10.1039/c8gc01960f.
[10] M.P. Pandey, C.S. Kim, Lignin depolymerization and conversion: a review of thermochemical methods, Chem. Eng. Technol. 34 (2011) 29–41, https://doi.org/10.1002/ceat.201000270.
[11] R. Behling, S. Valange, G. Chatel, Heterogeneous catalytic oxidation for lignin valorization into valuable chemicals: what results? What limitations? What trends? Green Chem. 18 (2016) 1839–1854, https://doi.org/10.1039/C5GC03061G.
[12] M. Wang, H. Shi, D.M. Camaioni, J.A. Lercher, Palladium-catalyzed hydrolytic cleavage of aromatic C−O bonds, Angew. Chemie - Int. Ed. 56 (2017) 2110–2114, https://doi.org/10.1002/anie.201611076.
[13] Q. Meng, M. Hou, H. Liu, J. Song, B. Han, Synthesis of ketones from biomass-derived feedstock, Nat. Commun. 8 (2017) 1–8, https://doi.org/10.1038/ncomms14190.
[14] M. Wang, O.Y. Gutiérrez, D.M. Camaioni, J.A. Lercher, Palladium-catalyzed reductive insertion of alcohols into aryl ether bonds, Angew. Chemie - Int. Ed. 57 (2018) 3747–3751, https://doi.org/10.1002/anie.201709445.
[15] J. He, C. Zhao, J.A. Lercher, Ni-catalyzed cleavage of aryl ethers in the aqueous phase, J. Am. Chem. Soc. 134 (2012) 20768–20775, https://doi.org/10.1021/ja309915e.
[16] J. He, L. Lu, C. Zhao, D. Mei, J.A. Lercher, Mechanisms of catalytic cleavage of benzyl phenyl ether in aqueous and apolar phases, J. Catal. 311 (2014) 41–51, https://doi.org/10.1016/j.jcat.2013.10.024.
[17] H. Jin, M.B. Ansari, S.E. Park, Chemoselective O-versus C-alkylation of substituted phenols with cyclohexene over mesoporous ZSM-5, Appl. Catal. A Gen. 472 (2014) 184–190, https://doi.org/10.1016/j.apcata.2013.12.025.
[18] G.D. Yadav, P. Kumar, Alkylation of phenol with cyclohexene over solid acids: Insight in selectivity of O- versus C-alkylation, Appl. Catal. A Gen. 286 (2005) 61–70, https://doi.org/10.1016/j.apcata.2005.03.001.
[19] P.A. Zapata, J. Faria, M.P. Ruiz, R.E. Jentoft, D.E. Resasco, Hydrophobic zeolites for biofuel upgrading reactions at the liquid-liquid interface in water/oil emulsions, J. Am. Chem. Soc. 134 (2012) 8570–8578, https://doi.org/10.1021/ja3015082.
[20] F. Anaya, L. Zhang, Q. Tan, D.E. Resasco, Tuning the acid-metal balance in Pd/ and Pt/zeolite catalysts for the hydroalkylation of m-cresol, J. Catal. 328 (2015) 173–185, https://doi.org/10.1016/j.jcat.2015.01.004.
[21] R.M. West, Z.Y. Liu, M. Peter, C.A. Gärtner, J.A. Dumesic, Carbon-carbon bond formation for biomass-derived furfurals and ketones by aldol condensation in a biphasic system, J. Mol. Catal. A Chem. 296 (2008) 18–27, https://doi.org/10.1016/j.molcata.2008.09.001.
[22] E.L. Kunkes, D.A. Simonetti, R.M. West, J.C. Serrano-Ruiz, C.A. Gartner, J.A. Dumesic, Catalytic conversion of biomass to monofunctional hydrocarbons and targeted liquid fuel classes, Science 80 (322) (2008) 417–421, https://doi.org/10.1126/science.1159210.
[23] D. Nguyen Thanh, O. Kikhtyanin, R. Ramos, M. Kothari, P. Ulbrich, T. Munshi, D. Kubička, Nanosized TiO_2—a promising catalyst for the aldol condensation of furfural with acetone in biomass upgrading, Catal. Today 277 (2016) 97–107, https://doi.org/10.1016/j.cattod.2015.11.027.
[24] P.A. Zapata, J. Faria, M. Pilar Ruiz, D.E. Resasco, Condensation/hydrogenation of biomass-derived oxygenates in water/oil emulsions stabilized by nanohybrid catalysts, Top. Catal. 55 (2012) 38–52, https://doi.org/10.1007/s11244-012-9768-4.
[25] C.J. Barrett, J.N. Chheda, G.W. Huber, J.A. Dumesic, Single-reactor process for sequential aldol-condensation and hydrogenation of biomass-derived compounds in water, Appl. Catal. B Environ. 66 (2006) 111–118, https://doi.org/10.1016/j.apcatb.2006.03.001.
[26] O. Kikhtyanin, D. Kubička, J. Čejka, Toward understanding of the role of Lewis acidity in aldol condensation of acetone and furfural using MOF and zeolite catalysts, Catal. Today. 243 (2015) 158–162, https://doi.org/10.1016/j.cattod.2014.08.016.
[27] A. Ungureanu, S. Royer, T.V. Hoang, D. Trong On, E. Dumitriu, S. Kaliaguine, Aldol condensation of aldehydes over semicrystalline zeolitic-mesoporous UL-ZSM-5, Microporous Mesoporous Mater. 84 (2005) 283–296, https://doi.org/10.1016/j.micromeso.2005.05.038.
[28] O. Kikhtyanin, V. Kelbichová, D. Vitvarová, M. Kubů, D. Kubička, Aldol condensation of furfural and acetone on zeolites, Catal. Today. 227 (2014) 154–162, https://doi.org/10.1016/j.cattod.2013.10.059.
[29] D.E. Resasco, B. Wang, S. Crossley, Zeolite-catalysed C–C bond forming reactions for biomass conversion to fuels and chemicals, Catal. Sci. Technol. 6 (2016) 2543–2559, https://doi.org/10.1039/C5CY02271A.
[30] K. Chen, J. Kelsey, J.L. White, L. Zhang, D. Resasco, Water interactions in zeolite catalysts and their hydrophobically modified analogues, ACS Catal. 5 (2015) 7480–7487, https://doi.org/10.1021/acscatal.5b02040.
[31] L. Zhang, K. Chen, B. Chen, J.L. White, D.E. Resasco, Factors that determine zeolite stability in hot liquid water, J. Am. Chem. Soc. 137 (2015) 11810–11819, https://doi.org/10.1021/jacs.5b07398.
[32] P.A. Zapata, Y. Huang, M.A. Gonzalez-Borja, D.E. Resasco, Silylated hydrophobic zeolites with enhanced tolerance to hot liquid water, J. Catal. 308 (2013) 82–97, https://doi.org/10.1016/j.jcat.2013.05.024.
[33] S. Wan, T. Pham, S. Zhang, L. Lobban, D. Resasco, R. Mallinson, Direct catalytic upgrading of biomass pyrolysis vapors by a dual function Ru/TiO_2 catalyst, AIChE J. 59 (2013) 2275–2285, https://doi.org/10.1002/aic.14038.
[34] X. Zhu, L.L. Lobban, R.G. Mallinson, D.E. Resasco, Bifunctional transalkylation and hydrodeoxygenation of anisole over a Pt/HBeta catalyst, J. Catal. 281 (2011) 21–29, https://doi.org/10.1016/j.jcat.2011.03.030.
[35] M. Guo, J. Peng, Q. Yang, C. Li, Highly active and selective RuPd bimetallic NPS for the cleavage of diphenyl ether C−O bond, ACS Catal. 812 (2018) 11174–11183.
[36] Q. Tan, G. Wang, L. Nie, A. Dinse, C. Buda, J. Shabaker, D.E. Resasco, Different product distributions and mechanistic aspcts of the hydrodeoxygenation of m-cresol over platinum and ruthenium catalysts, ACS Catal. 511 (2015) 6271–6283.
[37] Y. Yang, G. Lv, W. Guo, L. Zhang, Synthesis of mesoporous silica-included heteropolyacids materials and the utilization for the alkylation of phenol with cyclohexene, Microporous Mesoporous Mater. 261 (2018) 214–219, https://doi.org/10.1016/j.micromeso.2017.11.018.
[38] Q. Ma, D. Chakraborty, F. Faglioni, R.P. Muller, W.A. Goddard, T. Harris, C. Campbell, Y. Tang, Alkylation of phenol: a mechanistic view, J. Phys. Chem. A 110 (2006) 2246–2252, https://doi.org/10.1021/jp0560213.
[39] L. Ronchin, A. Vavasori, L. Toniolo, Acid catalyzed alkylation of phenols with cyclohexene: comparison between homogeneous and heterogeneous catalysis, influence of cyclohexyl phenyl ether equilibrium and of the substituent on reaction rate and selectivity, J. Mol. Catal. A Chem. 355 (2012) 134–141, https://doi.org/10.1016/j.molcata.2011.12.007.
[40] C. Zhao, W. Song, J.A. Lercher, Aqueous phase hydroalkylation and hydrodeoxygenation of phenol by dual functional catalysts comprised of Pd/C and H/La-BEA, ACS Catal. 2 (2012) 2714–2723, https://doi.org/10.1021/cs300418a.
[41] L. Ronchin, G. Quartarone, A. Vavasori, Kinetics and mechanism of acid catalyzed alkylation of phenol with cyclohexene in the presence of styrene divinylbenzene sulfonic resins, J. Mol. Catal. A Chem. 353–354 (2012) 192–203, https://doi.org/10.1016/j.molcata.2011.11.025.
[42] Y.S. Mahajan, R.S. Kamath, P.S. Kumbhar, S.M. Mahajani, Self-condensation of cyclohexanone over ion exchange resin catalysts: kinetics and selectivity aspects, Ind. Eng. Chem. Res. (2008) 25–33, https://doi.org/10.1021/ie061275b.